Development of Indium-Tin Oxide Thin Films on PAMAM Dendrimer Layers for Perovskite Solar Cells Application

Firdos Ali, Alecsander D. Mshar, Ka Ming Law, Xiao Li, A. J. Hauser, Shanlin Pan, Dawen Li, and Subhadra Gupta

Abstract Despite the dramatic progress that has been made in the power-conversion efficiency (PCE) of perovskite solar cells (PVSCs), there are still many obstacles to be overcome before these devices can be economically competitive in the photovoltaics market. One of the major hurdles in the commercialization of PVSCs is low stability, which severely limits the effective lifetime of the devices. One of the approaches to achieving higher stability and lifetime of PVSCs is improvement of PVSC film quality. In this paper, we have employed a PAMAM dendrimer layer to reduce the surface roughness of sputter-deposited indium-tin oxide (ITO) films, which were then used in the fabrication of PVSCs. A PAMAM-8 dendrimer layer was deposited by dip-coating the substrates in 25 mL of a 1 μM PAMAM-8 ethanol solution before ITO deposition. X-ray refractivity (XRR) was used to verify the PAMAM layer on the substrate. ITO films of 150 nm thickness were then deposited onto the PAMAM layer using DC magnetron reactive sputtering. The surface roughness, sheet resistance, and transmissivity of the ITO films were optimized by varying the parameters of the sputtering process. Atomic force microscopy (AFM) was used to measure the surface roughness of the ITO films with and without PAMAM dendrimer layer. A root-mean-square (RMS) film roughness of 1.6 nm, sheet resistance of 21 Ω/ϒ, and transmissivity of > 91% at a wavelength of 400–700 nm were obtained after optimization.

F. Ali (✉) · S. Gupta
Department of Metallurgical and Materials Engineering, The University of Alabama, Tuscaloosa, AL 35487, USA
e-mail: mfali@crimson.ua.edu

A. D. Mshar · D. Li
Department of Electrical and Computer Engineering, The University of Alabama, Tuscaloosa, AL 35487, USA

K. M. Law · A. J. Hauser
Department of Physics and Astronomy, The University of Alabama, Tuscaloosa, AL 35487, USA

X. Li · S. Pan
Department of Chemistry, The University of Alabama, Tuscaloosa, AL 35487, USA

© The Minerals, Metals & Materials Society 2023

S. Alam et al. (eds.), *Energy Technology 2023*, The Minerals, Metals & Materials Series,
https://doi.org/10.1007/978-3-031-22638-0_3

Keywords ITO · G8 PAMAM dendrimer · Sputtering · Sheet resistance · Transmittance

Introduction

Perovskite solar cells (PVSCs) have recently garnered significant attention in many research communities. Current single-junction PVSCs rival the power-conversion efficiency (PCE) of Si cell designs and are generally cheaper and easier to fabricate than similarly performing Si cells [1–6]. One of the major roadblocks to further adoption of PVSCs is their low stability compared to Si cells—PVSCs do not perform well in ambient conditions and quickly deteriorate [7–9]. Since PVSCs are composed of several layers of different materials that are sequentially deposited, the performance and stability of these devices are heavily influenced by the quality of these layers and their interfaces. In this paper, we have developed processes to improve the film quality of sputter-deposited indium-tin oxide (ITO) for the synthesis of efficient PVSCs.

ITO is a transparent, conductive oxide that is widely used in many different devices. ITO is commonly used in PVSCs as a transparent transport layer. As a transport layer, the ITO film must have both high transparency and high conductivity to reduce parasitic loss in the device. The improved surface roughness of these ITO thin films will (1) improve the PCE of solar cell devices that utilize this material and (2) improve the interfacial structure of layered devices, contributing to better overall stability. In this paper, we have optimized ITO thin films by three metrics: resistivity, transmissivity, and surface roughness. These film properties were optimized by varying the parameters of the film deposition technique and post-deposition treatment. The ITO films were deposited by reactive DC magnetron sputtering using a Sputtered Films, Inc. Planetary Sputtering System. The deposition parameters of sputter power, sputter time (film thickness), reactive gas flow rate, and post-deposition annealing time were all varied to produce an optimal ITO thin film for use in PVSCs. In addition to the deposition parameters, a pre-deposition PAMAM dendrimer layer was also employed to further reduce the surface roughness of the ITO films [10]. The ITO films were then characterized by several different methods: a 4-point probe was used to measure the sheet resistance of the films; a profilometer and ellipsometer were used to measure the film thickness; an atomic force microscope (AFM) was used to measure the film surface roughness; and an X-ray diffractometer was used to perform X-ray reflectivity (XRR) measurements in order to detect the presence of the PAMAM dendrimer layer.

Experimental

Eighth generation (G8) PAMAM amine-terminated dendrimer (Dendritech, Midland, MI) in a 5% w/w methanol solution was used without any additional processing.

Ethanol (Purity > 99.99) (Sigma-Aldrich Inc, St. Louis, MO) was used to prepare a 1 μM solution of the G8 amine-terminated dendrimer. 25 mL of the 1 μM dendrimer solution was used to fabricate a dendrimer layer on glass substrates with the dimensions of 25 × 25 × 1 mm [11]. The glass substrates were fully submersed in an ethanol (EtOH) and potassium hydroxide (KOH) solution for 1 h to remove organic and inorganic impurities. The substrates were then rinsed with de-ionized (DI) water (18 MΩ) and isopropanol and dried under a steady stream of nitrogen gas. The substrates were subsequently cleaned using a UV/O_3 cleaner (UV/O_3-Cleaner model 42, Jelight Company, Irvine, CA) for 1 min to remove any adsorbed hydrocarbon contaminants. Finally, the substrates were fully submerged in the 1 μM PAMAM dendrimer ethanol solution for over 15 h. After removing the glass substrates from the solution, they were thoroughly rinsed in pure ethanol and then dried under a steady stream of nitrogen gas. The final samples were stored in a desiccator to prevent decomposition of the dendrimer layer. All the steps described above are shown in Fig. 1.

Sputter deposition of the ITO films was done using a sputter up SFI Shamrock Planetary Sputtering System in the Microfabrication Facility at the University of Alabama. The sputter target used was a 95% dense pressed powder compact of In_2O_3:SnO_2 90:10 wt.%. First, the following ITO sputter deposition conditions were optimized with respect to resistivity and transmissivity: 200–700 W DC sputter power and 0–2.0 sccm oxygen flow with a total (argon + oxygen) flow rate of 50 sccm. The ITO sputter depositions were all done at a 2.71 mTorr process pressure. Depositions over a similar range of conditions were carried out on both silicon wafers and glass substrates in the same batch. The glass substrates and silicon wafers were first rinsed

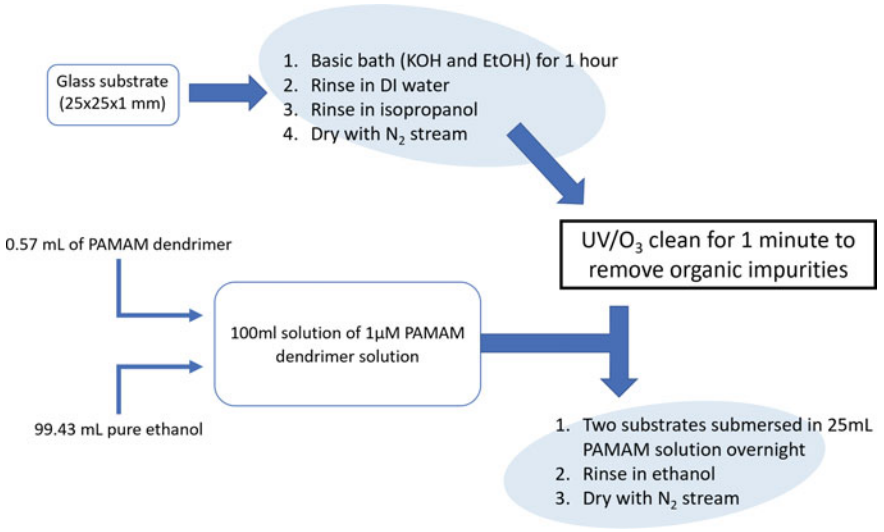

Fig. 1 Flow chart of the PAMAM layer deposition process

with 100% isopropanol to remove any unbound impurities and then dried in a stream of nitrogen gas.

Transmission measurements were performed using UV–VIS spectrophotometers over a range of 400–700 nm wavelength. Baseline corrections were performed using a blank glass substrate, and the scan rate was 600 nm/min. Sheet resistance measurements were performed using four-point probes at two different facilities. Thickness measurements were done using a Veeco Dektak profilometer. Surface roughness measurements were done using a Digital Instruments Dimension 3100 AFM in tapping-mode. XRR measurements were done using a Rigaku SmartLab X-ray diffractometer in parallel-beam mode.

Results and Discussion

Reactive Gas Flow Rate

It has been shown that the sheet resistance and transmittance of ITO films are directly related to the oxygen flow rate during the sputtering process [12]. ITO thin films were sputtered at different oxygen flow rate percentages to optimize for resistance and transmittance. Figure 2 shows the sheet resistance of several 150 nm-thick ITO films deposited at various oxygen flow rates, at a power of 700 W and a total gas flow rate of 50 sccm at room temperature. As oxygen flow rate is increased from 0%, the sheet resistance first decreased to 54 Ω/ϒ at an oxygen flow rate of 1.0% and then increased with an increasing oxygen flow rate until saturating at around 83–85 Ω/ϒ near 2.0%. The above supports the fact that, since the conductivity of ITO films strongly depends on charge carrier concentration such as Sn^{4+} and oxygen vacancies on the substitution sites of In_2O_3, the conductivity of an ITO film can be increased by depositing the films in a low oxygen environment [13]. Figure 3 shows the transmittance of several ITO films over a wavelength range of 400–700 nm. As the flow of oxygen increases, transmittance of the films also increases. Similar behavior was observed with other oxygen flow percentages which is not shown in Fig. 3.

Film Thickness

Figure 4 shows how the sheet resistance varies with ITO film thickness. Initially, the sheet resistance decreases as the film thickness increases. As the film thickness increases beyond 150 nm, the sheet resistance starts to increase. It is known that the transmissivity of the ITO films strongly depends on film thickness—thicker films have lower optical transmission due to increased optical path and optical scattering. This is demonstrated in Fig. 5, which shows the decrease of optical transmittivity as thickness increases.

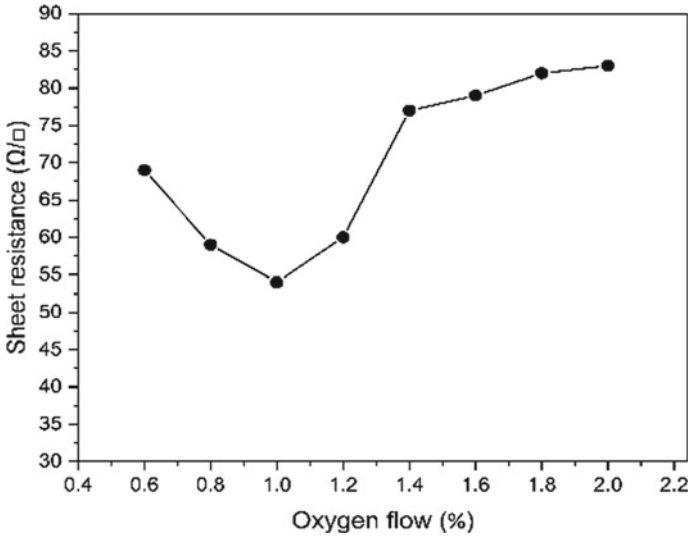

Fig. 2 ITO film room temperature sheet resistance with increasing oxygen flow rate. Sheet resistance reaches a minimum value at 1.0% flow rate

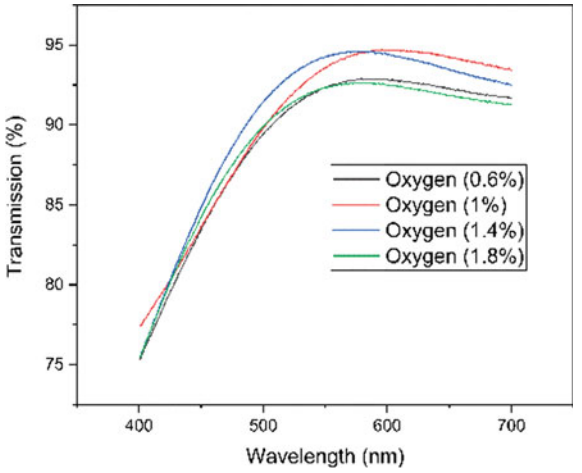

Fig. 3 ITO film optical transmission with increasing oxygen flow rate

Annealing Conditions

Figure 6 shows how the sheet resistance varies with annealing conditions. Three samples were deposited simultaneously with identical parameters: 700 W deposition power, 15 min deposition time, and a 1% oxygen flow rate. All anneals were done for 5 min at 180 °C. The first sample shows a sheet resistance of 54 Ω/ϒ without

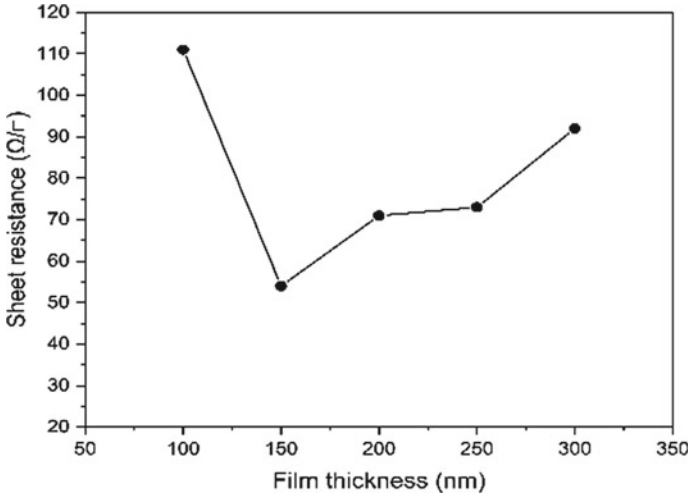

Fig. 4 ITO film room temperature sheet resistance with increasing film thickness

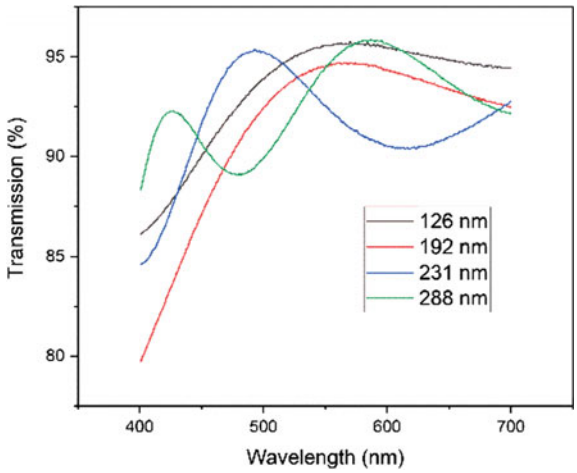

Fig. 5 ITO film optical transmission with increasing film thickness

annealing. The second sample went through both pre- and post-deposition annealing, which reduced the sheet resistance from 54 to 29 Ω/ϒ. The final sample was only post-annealed, which showed the lowest sheet resistance of 21 Ω/ϒ. We postulate that the increase in temperature immediately before the deposition increased residual stress due to a mismatch in thermal expansion coefficients between the substrate and the films.

Figure 7 shows the sheet resistance of the films as the post-annealing time was changed. The sample that was annealed for 5 min yields the lowest sheet resistance

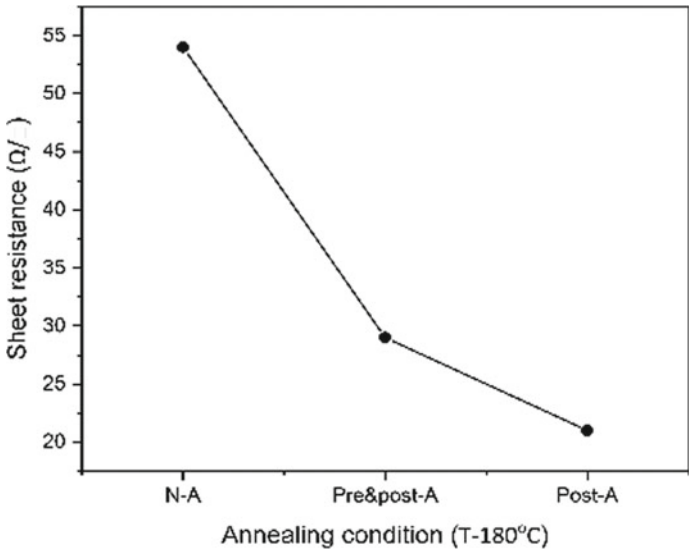

Fig. 6 ITO film room temperature sheet resistance of samples that underwent different annealing conditions

of 21 Ω/ϒ. As the annealing time is increased beyond 5 min, the sheet resistance of the film begins to increase. The data suggests that post-annealing times lower than 5 min may not have been sufficient for good crystallinity, hence leading to poor film quality and increased sheet resistance. In addition, Fig. 8 shows the transmittance of the ITO films at wavelengths between 400 and 700 nm for films with different post-annealing durations. The sample annealed for 5 min at 180 °C shows the best transmittance.

Deposition Power

The DC sputtering power was varied between 200 and 700 Wfor the ITO deposition. An optimum ITO film thickness of 150 nm was chosen from the results shown above. The final thickness of the deposited films was kept constant by varying the deposition time according to the deposition power. The relationship between sheet resistance and sputtering power is shown in Fig. 9, which depicts an overall downward-sloped trend, with the lowest sheet resistance observed being 21 Ω/ϒ at a deposition power of 700 W. This may be attributed to the higher deposition rate and ion-energy during the deposition process, both of which likely increased the film uniformity and crystallinity.

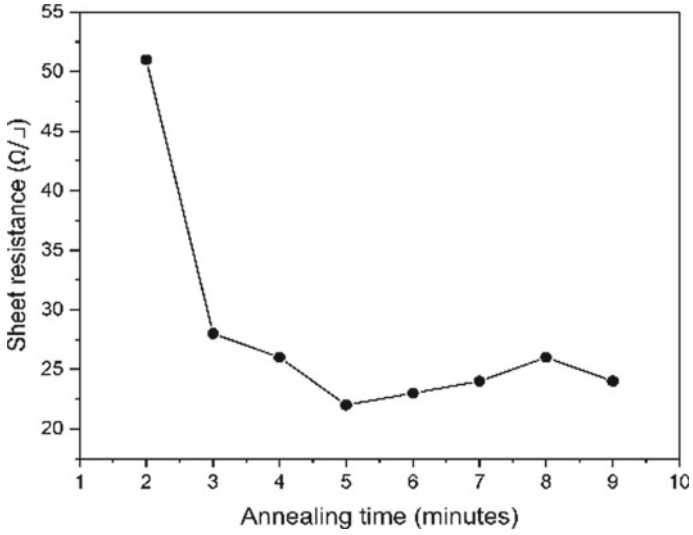

Fig. 7 ITO film room temperature sheet resistance with increasing post-annealing time

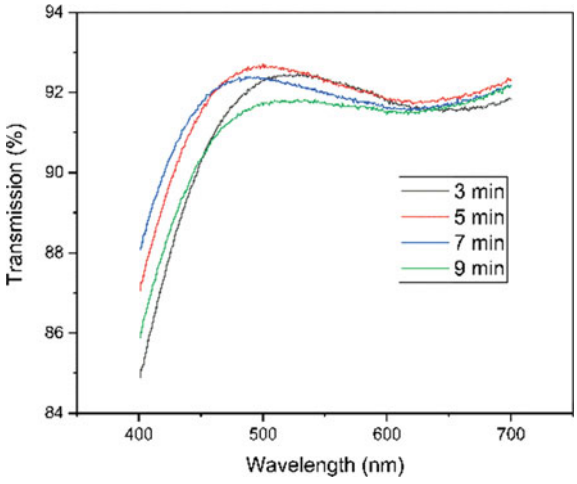

Fig. 8 ITO film optical transmission spectra at different post-annealing times

PAMAM Dendrimer Layer

ITO thin films were deposited on a G8 PAMAM dendrimer layer on a glass substrate. The successful deposition of the dendrimer layer was verified by XRR, as shown in Fig. 10. The layer thickness was calculated as follows:

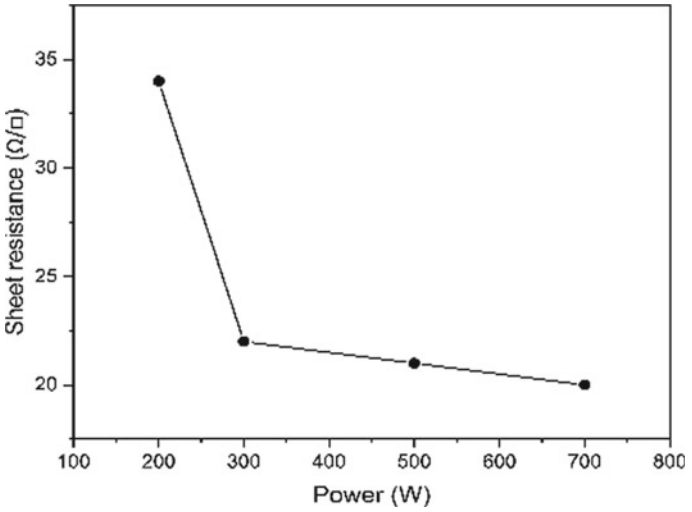

Fig. 9 ITO film room temperature sheet resistance with increasing sputtering power

$$2D\sqrt{\sin^2(\theta_m) - \sin^2(\theta_c)} = m\lambda$$

The critical angle was identified to be at 0.46°, along with three thickness fringes at 0.68°, 1.11°, and 2.14°. The presence of XRR thickness fringes indicates two abrupt interfaces, which we attribute to the substrate/dendrimer layer interface and the layer surface. If this were the case, then the angular spacing between each adjacent pair of fringes would give the distance between the interfaces, i.e. layer thickness,

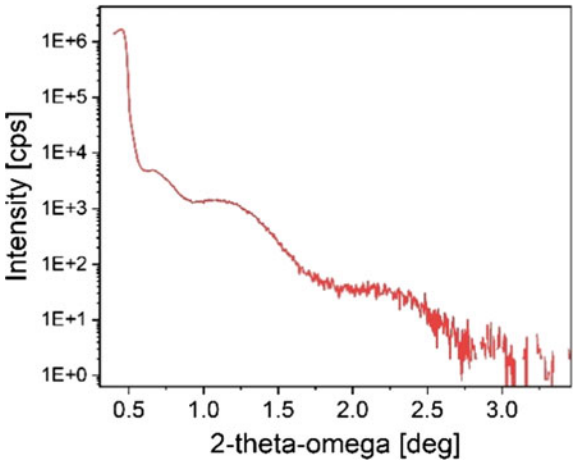

Fig. 10 X-ray reflectivity spectrum of PAMAM layer on glass substrate

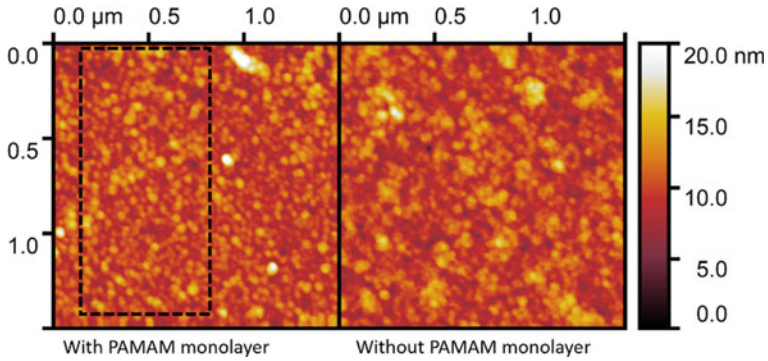

Fig. 11 AFM image of ITO thin film on PAMAM dendrimer layer (left) and without PAMAM dendrimer layer (right). The film deposited on PAMAM dendrimer layer has an RMS surface roughness of 1.6 nm, while the film deposited on bare glass substrate has a roughness of 3.2 nm

which is approximately 4 nm. While 3 is a small number of fringes, note that the number of fringes is not only limited by the film layer interface quality, but also by the instrument noise level. A thicker dendrimer layer would have shown more fringes.

Figure 11 shows AFM images of ITO thin films with and without an underlying dendrimer layer. These measurements show that both films generally have no height variations larger than 20 nm [14]. The RMS surface roughness of the ITO sample deposited on the dendrimer is 1.6 nm, while the surface roughness of the sample without a dendrimer layer is 3.2 nm. The ITO film deposited on a dendrimer layer demonstrated marginally lower surface roughness than the ITO film that was deposited directly onto the glass substrate. This difference may be attributed to the layer's ability to facilitate and form nucleation sites for the deposited ITO film. This leads to finer grains and a smoother film, though the improvement in surface roughness is not significant.

Figure 12 shows that the sheet resistance of an ITO film is slightly higher when deposited on a dendrimer layer-coated glass substrate, since the PAMAM dendrimer is insulative. The sample prepared with a dendrimer layer shows slightly higher transmission when compared with the film without a dendrimer layer. This enhancement in transmission is attributed to the index-matching provided by the PAMAM dendrimer layer.

Conclusion

The sputter deposition process of ITO films was optimized for use in the fabrication of efficient, stable PVSCs. The film qualities of sheet resistance, transmission, and

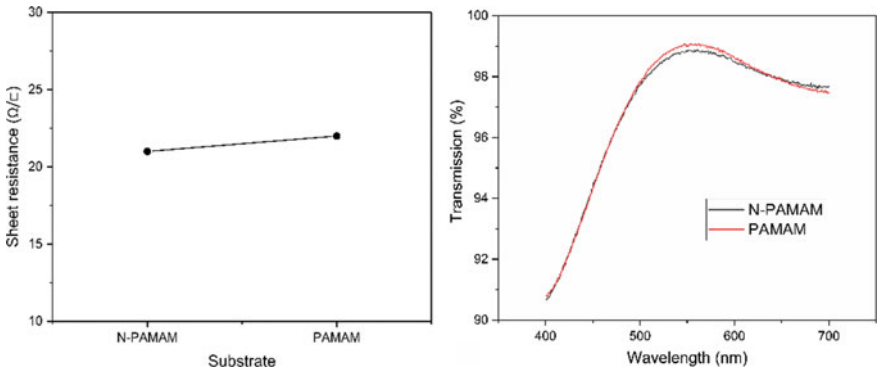

Fig. 12 Room temperature sheet resistance (left) and optical transmission (right) comparison of ITO films with and without PAMAM layer

surface roughness were improved by varying the deposition conditions and introducing other film and substrate treatments. A G8 PAMAM dendrimer layer was used as interfacial layer to improve the surface roughness of the ITO film. The surface roughness of these films was decreased from 3.2 nm without a dendrimer layer to 1.6 nm with a dendrimer layer. By varying the sputter deposition parameters and annealing treatments, a sheet resistance of 21 Ω/ϒ was achieved. In addition to low resistivity, a high transmissivity above 91% was achieved in the wavelength range of 400–700 nm.

Acknowledgements We acknowledge NSF ECCS-2053954 for support. The authors would like to acknowledge Dr. Shane Street for valuable advice.

Conflict of Interest The authors have no conflicts of interest to disclose.

References

1. Best research-cell efficiency chart. In: NREL.gov. https://www.nrel.gov/pv/cell-efficiency.html. Accessed 4 Oct 2022
2. Zhao Y, Zhu P, Wang M et al. (2020) A polymerization-assisted grain growth strategy for efficient and stable perovskite solar cells. Adv Mater 32:1907769
3. Jung EH, Jeon NJ, Park EY, Moon CS, Shin TJ, Yang T-Y, Noh JH, Seo J (2019) Efficient, stable and scalable perovskite solar cells using poly(3-hexylthiophene). Nature 567:511–515
4. Yoo JJ, Wieghold S, Sponseller MC et al. (2019) An interface stabilized perovskite solar cell with high stabilized efficiency and low voltage loss. Energy Environ Sci 12:2192–2199
5. Zhu H, Liu Y, Eickemeyer FT et al. (2020) Tailored amphiphilic molecular mitigators for stable perovskite solar cells with 23.5% efficiency. Adv Mater 32:1907757
6. Min H, Kim M, Lee S-U, Kim H, Kim G, Choi K, Lee JH, Seok SI (2019) Efficient, stable solar cells by using inherent bandgap of α-phase formamidinium lead iodide. Science 366:749–753

7. Zhang Y, Hu X, Chen L, Huang Z, Fu Q, Liu Y, Zhang L, Chen Y (2016) Flexible, hole transporting layer-free and stable CH 3 NH 3 PBI 3/PC 61 BM planar heterojunction perovskite solar cells. Org Electron 30:281–288
8. Snaith HJ, Abate A, Ball JM, Eperon GE, Leijtens T, Noel NK, Stranks SD, Wang JT-W, Wojciechowski K, Zhang W (2014) Anomalous hysteresis in perovskite solar cells. J Phys Chem Lett 5:1511–1515
9. Gupta V, Lucarelli G, Castro-Hermosa S, Brown T, Ottavi M (2020) Investigation of hysteresis in hole transport layer free metal halide perovskites cells under dark conditions. Nanotechnology 31:445201
10. Gupta S, Ada E (2005) Optimization of process parameters to achieve high quality as-deposited indium-tin oxide films for display applications. J Vac Sci Technol A Vac Surf Films 23:1173–1179
11. Thunuguntla R (2006) Effect of dendrimer mediation and rapid thermal annealing on indium-tin oxide thin films. Thesis
12. Sohn MH, Kim D, Kim SJ, Paik NW, Gupta S (2003) Super-smooth indium–tin oxide thin films by negative sputter ion beam technology. J Vac Sci Technol A Vac Surf Films 21:1347–1350
13. Wong FL, Fung MK, Tong SW, Lee CS, Lee ST (2004) Flexible organic light-emitting device based on magnetron sputtered indium-tin-oxide on plastic substrate. Thin Solid Films 466:225–230
14. Chu JB, Huang SM, Zhu HB, Xu XB, Sun Z, Chen YW, Huang FQ (2008) Preparation of indium tin oxide thin films without external heating for application in solar cells. J Non-Cryst Solids 354:5480–5484